Scientific paper

## Fabrication of Zirconium Silicate Reinforced Superhydrophobic Coating for the Evaluation of Corrosion-Resistance

## Mubarak Ali Muhamath Basha<sup>1,\*</sup> and Sathiya Srinivasan<sup>1</sup>

Department of Chemistry, Chikkaiah Naicker College, Erode-638004. Tamilnadu, India

\* Corresponding author: E-mail: mubarakscience@gmail.com

Received: 07-19-2021

## **Abstract**

The present work investigates on anodisation of aluminium in 1.0 M sodium oxalate and methodically evaluates the influence of zirconium silicate as an additive. The effect of additive upon structure, morphology, micro hardness and composition of the coating formed under various anodising conditions has been examined comprehensively. The surface of the coating was modified by stearic acid and its immersion time was optimized. The dependence of surface morphology, kinetic parameters, and microstructural characteristics of the coating on electrolyte /additive concentration, anodising time, and the temperature has also been inspected. X-ray diffraction (XRD), Scanning Electron Microscopy (SEM) combined with EDAX studies indicates the beneficial role of zirconium silicate towards the formation of crystalline coating with improved corrosion-resistant characteristics. The static water contact angle on the surface-modified coatings was  $122^{\circ} \pm 0.4^{\circ}$ . This contact angle of super hydrophobic coating has been improved by KOH treatment (152.76°  $\pm$  0.4°) which is obtained under optimized conditions exhibit the corrosion resistance (1.68 × 10<sup>8</sup>  $\Omega$  cm<sup>-1</sup>) which is nearly 8 times higher than that of bare aluminium (8.36 × 10<sup>1</sup>  $\Omega$  cm<sup>-1</sup>). The efficacies of the surface-modified coatings against bacteria that are commonly encountered in marine (Desulfovibrio desulfuricans) and medical applications (Staphylococcus aureus and Escherichia coli) are also demonstrated.

Keywords: Anodisation; aluminium; sodium oxalate; corrosion resistance.

## 1. Introduction

Aluminium is selected for their optimal combination of physical and mechanical properties. 1 Another benefit, which may be just as significant from an environmental standpoint, is that aluminium components may be recycled with relatively little energy use.<sup>2</sup> In damp environments, however, this thin layer is reactive and susceptible to corrosion and contamination.<sup>3</sup> Anodisation of aluminium is a well-established and easy method in comparison with micro-arc discharge oxidation (MDO), gas flame spray, plasma thermal spray, physical vapour deposition, and high-temperature glass enamelling methods to progress the applicability of aluminium.<sup>4-5</sup> Since, anodisation is an electrochemical process, its conditions (voltage, time, temperature) and composition of electrolytes together, play a central role in the characteristics of the coating.

In this connection, numerous investigations devoted to exploring the relationship between the composition

of the electrolytes (e.g., sulfuric acid, chromic acid, phosphoric acid, or oxalic acid) and anodic behaviour of aluminium. However, because the acid molecules confined within the holes may cause more corrosion, the porous type oxide layer is not desirable for corrosion prevention.<sup>6</sup> To resolve this issue, the weak electrolytes are preferred. To enhance further the corrosion resistance, abrasion resistance, and electrical insulation of the oxide coating and to increase the coating thickness, additive salts have been added into the electrolytic solution as investigated by numerous studies.<sup>7–9</sup> Scarcely, reports are available upon the use of zirconium silicate as an additive for anodisation of aluminium, except for our earlier study on aluminium anodisation with Lithium sulphate-zirconium silicate bath, 10 which illustrated that significant enhancement in corrosion protection and micro hardness behaviour of nanocomposite coatings.

Super hydrophobicity, found on many natural surfaces, the most classic example being the lotus leaf, has inspired researchers around the world for its unique charac-

teristics such as self-cleaning,11 water repellence,12 anti-icing, 13 anti-corrosion, 14 and oil-water separation. 15 The presence of a low energy layer over a rough hierarchical structure is crucial for constructing a hydrophobic surface. 16 So far, a large number of approaches have been successfully used to develop superhydrophobic surfaces, including chemical vapour deposition,<sup>17</sup> chemical etching, 18 sol-gel, 19 solution immersion, 20 hydrothermal synthesis,<sup>21</sup> and laser fabrication,<sup>22</sup> etc., Anodisation is an effective technique to fine-tune the surface morphology trough constructing superhydrophobic surface.<sup>23</sup> Preparation of the superhydrophobic surface of the aluminium substrate by anodisation in phosphoric acid followed by low-temperature plasma treatment is reported.<sup>24</sup> Investigation about a superhydrophobic surface on aluminium alloy via anodising in an electrolyte consisting of sulfuric acid, oxalic acid, and sodium chloride, followed by polypropylene coating is also attempted successfully.<sup>25</sup> Heretofore, researchers coated an anodized aluminium alloy surface with RF-sputtered polytetrafluoroethylene to generate a superhydrophobic surface.<sup>26</sup> In terms of real-world applications, fabricating hydrophobic aluminium alloy surfaces with superior corrosion resistance and chemical stability is critical.27

In this regard, herein we report the anodic behaviour of aluminium in the presence and absence of a zirconium silicate additive using sodium oxalate as an electrolyte. The parameters such as the concentration of the electrolyte/additive, voltage, temperature, etc., were studied to establish the correlation with growth kinetic parameters namely thickness and growth rate. The anodic coating formed which was immersed in stearic acid for surface modification and the immersion time was varied for optimization. We have also studied the mechanical properties, microstructural characterisation, chemical composition, and electrochemical corrosion behaviour of the coating which is prepared with and without the addition of zirconium silicate additive in non-conventional weak electrolyte namely sodium oxalate followed by surface modification of anodic coating. Further, we have also carried out the corrosion behaviour of anodic layer and surface modified anodic layer formed under various experimental conditions are determined by Tafel polarization and electrochemical impedance spectroscopy (EIS) analyses.

## 2. Experimental Methods

### 2. 1. Materials

Sodium oxalate, zirconium silicate, sulphuric acid, sodium chloride, chromic acid, phosphoric acid, per chloric acid, ethanol, stearic acid, and acetone were purchased from Aldrich chemicals (Aldrich, India). All of the chemicals used were analytical grade and were used as received. Deionized water was used in all of the studies.

## 2. 2. Preparation of Anodic Coating

High purity aluminium (99.999% pure, AL104, Mettler-Toledo International. Inc.) The plate of thickness 0.5 mm was used for this investigation. Surface pre-treatment is a successive step involved in the process of anodisation. The surface pre-treatment process was accomplished by following the procedure reported elsewhere. Aluminium was cleaned and degreased with the use of ultrasonicator by using acetone, water and ethanol as a medium. The surface cleaned aluminium samples were subjected to the thermal annealing process at 450 °C for 30 min.

The etching process is performed by immersing the samples in 5% sodium hydroxide for 2 min at room temperature (35°  $\pm$  1 °C) to cast off the native oxide layer. The resulted aluminium samples were subjected to electro polishing in a mixture consists of perchloricacid:ethanol (1: 3) under an applied voltage of 20 V, which is maintained for 3 min. The pre-treated samples thus obtained were used for anodising studies in a two-electrode configuration using a direct current power supply (Aplab Model: 05 A/30 V and 0-1 A/120 V) and we determined the weight of every specimen. Graphite sheet is used as a cathode and the sample to be anodised acts as an anode in an electrolytic bath comprising 1.0 M sodium oxalate with and without zirconium silicate additive. The anodised coatings obtained from the bath containing zirconium silicate concentration of 0, 0.1 g/L, 0.2 g/L, 0.3 g/L to 0.4 g/L are designated as SO, Zr1, Zr2, Zr3 and Zr4 respectively. Anodised specimens were cleaned with de-ionized water pursued by drying in the N<sub>2</sub> atmosphere and their weight is determined. 1 cm<sup>2</sup> working surface is used for the study and the rest of the surface was insulated using an epoxy resin. All the experimental studies were carried out in aerated and stirred conditions. These experiments were repeated in triplicate to acquire accurate results. The anodic coating formed under an optimized condition was immersed in stearic acid for surface modification at various time intervals such as 15 and 30 min. These two samples are designated as SA1 and SA2. The steps involved in the process is schematically depicted in Scheme S1.

## 2. 3. Characterisation of Anodic Coating

The crystalline nature of the coating was examined using a Philips X-Pert X-ray Diffractometer (XRD) with the use of CuKa radiation of wavelength,  $\lambda = 1.54$  Å with Step Size [° 2 $\theta$ ] 0.0300. Scanning Electron Microscope (SEM, FEI - QUANTA-FEG 250, Japan) is used to examine the surface morphologies of the coating. Field emission scanning electron microscope and energy-dispersive X-ray spectroscopic studies were carried out to analyse the microstructure and elemental composition of the coatings. Vickers micro hardness indenter is used to quantify the micro hardness of the specimen. (Tester MH6, USA). Thickness tester (Touchstone1) is employed for measuring the coating thickness non-destructively. Contact Angle associated with SA1 and SA2 surfaces was measured with a

contact angle measuring system (OCA20, Data physics Corporation, Germany) under ambient temperature. All the measurements were conducted at five positions on each sample with 4  $\mu$ L DI water droplets. To evaluate the durability of the Zr3, SA1 and SA2 samples, the influences of exposure to air at room temperature (35°  $\pm$  1 °C) were systematically investigated.

# 2. 4. Preparation of Superhydrophobic Coating

To examine the corrosion resistance of the superhydrophobic coatings were carried out for optimized Zr3 (Zirconium silicate), SA1 (stearic acid) and SA2 (stearic acid & KOH) samples for comparison. The SA1 was prepared by using the Zr3 sample immersed in stearic acid 3g/L for 15 min. To further enhance the super hydrophobicity, KOH treatment was applied to prepare by using the SA1 immersed in stearic acid 10 g/L KOH for 30 min (SA2).

## 2. 5. Evaluation of Corrosion Resistance

Tafel polarisation investigations and electrochemical impedance spectroscopy (EIS) in 3.5 percent NaCl (using an electrochemical workstation (600TM Potentiostat/ Galvanostat, Inc.) are used to examine the coatings' electrochemical corrosion behaviour. These studies were executed in the three-electrode configuration that consists of Ag/ AgCl/saturated KCl as a reference electrode, a platinum wire as a counter electrode, and aluminium as a working electrode. Fully aerated conditions are maintained during the experiments. Tafel polarisation studies were performed by applying potential in the range of +2 V to -2 V with a scan rate of 1 mV/s. Using the method of extrapolation of anodic and cathodic sections, current density associated with corrosion (I<sub>corr</sub>) and the resistance offered for charge transfer reaction (R<sub>P</sub>) is determined and tabulated as shown in Table. 1. R<sub>p</sub> is determined with the use of Stern-Geary equation as follows,<sup>29</sup>

$$R_{P} = \frac{b_{a}b_{c}}{2.303 \, I_{corr} (b_{a} + b_{c})} \tag{1}$$

Where in  $I_{corr}$  signifies corrosion current density, cathodic/anodic Tafel constants as  $(b_a$  and  $b_c$ ).  $I_{corr}$  and  $E_{corr}$  are obtained from the intercept of Tafel slopes. EIS plots are recorded at frequencies between 100 kHz and 0.01 Hz with 12 points per decade. The amplitude of the sinusoidal potential signal was set as 5 mV. The impedance spectra obtained were analysed by fitting with an appropriate Randel's equivalent circuit.

### 2. 6. Marine Bacterial Studies

The marine bacteria used in this study were the sulphate reducing strains of Desulfovibrio desulfuricans

(ATCC#14563). The bacterium was cultured at 37 °C in a modified Postgate's C medium used for enrichment culture, which contained 35 g NaCl, 0.5 g KH<sub>2</sub>PO<sub>4</sub>, 0.06 g CaCl<sub>2</sub> 2H<sub>2</sub>O, 2 g MgSO<sub>4</sub> 7H<sub>2</sub>O, 1 g yeast extract, 0.004 g FeSO<sub>4</sub> 7H<sub>2</sub>O, and 0.3 g sodium citrate in 1 L deionized water. The medium was autoclaved at 121°C and 20 psi for 15 min.<sup>30-31</sup> after the stipulated period (7 days), the SA1 and SA2 were washed twice with phosphate-buffered saline (19 PBS, pH 7.4). The cells were detected by live/dead staining. 200 mL of dye mixture (100 mL acridine orange, green fluorescence in live cells, and 100 mL ethidium bromide, red fluorescence in dead cells in distilled water) was mixed with 2 mL cell suspension in a well plate. The suspension was studied right away using an Olympus Ti-Eclipse inverted fluorescence microscope to record the data under the magnification of 400 x of the instrument.

## 3. Results and Discussion

## 3. 1. Anodising Process Optimization Studies

A methodical comprehensive evaluation of the influence of the composition of the additive into the electrolyte, period of anodisation process, and anodising temperature upon morphology and kinetics of the coating has been carried out to comprehend the fundamental mechanism behind the formation of the highly corrosion-resistive layer. To recognize the role of additive towards tuning the microstructural features, morphology, micro-hardness, and corrosion resistance of the coating was carried out in sodium oxalate in the presence and absence of zirconium silicate. The optimal concentration of sodium oxalate was kept as 1.0 M.

## 3. 1. 1. Effect of Zirconium Silicate Concentration Additive

The formation and properties of the coating are greatly manipulated by the concentration of zirconium silicate as illustrated by Fig S1a, wherein the concentration of zirconium silicate is varied from 0.1 g/L to 0.4 g/L in 1.0 M sodium oxalate at constant voltage of 55 V and temperature (35°  $\pm$  1° C). This behavior could be explained due to the existence of two competing reactions, namely oxide coating growth and its dissolution. Based on an earlier study, a sequence of reactions occurs during the anodisation process together with the combination of metal ions with OH and SiO<sub>3</sub> to form Al (OH)<sub>3</sub> and Al<sub>2</sub> (SiO<sub>3</sub>)<sub>3</sub>. In the current report, the presence of zirconium silicate (0.3 g/L) leads to develop the coating with a high thickness (82  $\mu$ m).

The coating obtained using sodium oxalate without additive results in poor growth performance (thickness: 70  $\mu$ m; growth rate: 0.9  $\mu$ m/min). From Fig. S1a, it is intended that the zirconium silicate concentration directly impacts the thickness (growth rate: 1.2  $\mu$ m/min) of the coating.

Therefore, to throw the light about the kinetics of the coating, zirconium silicate concentration is varied from 0.1 g/L to 0.4 g/L (0.1 g/L, 0.2 g/L, 0.3 and 0.4 g/L) and exploration is directed towards to develop the coating uniformly. When the concentration of zirconium silicate increases from 0.1 g/L to 0.4 g/L, the silicate ion concentration increases and these ions interact with  $Al_2$  (SiO<sub>3</sub>)<sub>3</sub>. The credible rationale behind this performance is strongly related to the presence of zirconium silicate additive resulting in non-uniform cooling near the anode surface.

The coating thickness has been increased when zirconium silicate is added into the sodium oxalate solution. At this juncture, anodic coating with more thickness is favoured rather than thin oxide coating and the incorporation of  $\rm ZrO_2$  into the oxide layer is high. So the thickness of the coating also upsurges. Owing to pitting attack on pre-formed barrier oxide which is formed under the low zirconium silicate concentration (< 0.1 g/L), the surface becomes non-uniform. However, when the additive concentration exceeds optimum, the dissolution rate of the coating by anodisation dominates over its formation.

When the concentration of zirconium silicate is increased beyond the optimal level (0.3 g/L) ease of access and inner movement of the oxygen ions  $(O^{2-})$  or hydroxide ions (OH-) towards the Al/Aluminium oxide interface improves, which react with  $Al^{3+}$  ions that are shifted around outwards from aluminium surfaces. This tendency results in declined growth parameters because the entire specimen is being surrounded by an oxide layer. From the results, it is inferred that the rate of deposition, morphological properties, and thickness of the coating which strongly depends on zirconium silicate additive concentration. This observation is analogous to previous studies wherein aluminium anodisation is carried out in weak electrolyte with the addition of silicate material.  $^{13-14}$ 

### 3. 1. 2. Effect of Anodisation Voltage

Fig. S1b depicts the influence of anodisation voltage on growth kinetics which is evaluated by carrying out anodisation at constant temperature and optimized zirconium silicate additive concentration on varying voltage from 45 V to 65 V. From the results, it can be construed that the thickness and growth rate characteristics go linearly with voltage up to 55 V and started to decline after that. Since the oxidation occurs at a slow rate, the coating thickness (62 µm) at a lower voltage (45 V), has been formed with deprived mechanical properties. When voltage maintained is optimal (55 V), the system can afford more driving force for the ions needed for the growth, and it makes it likely to increase the incorporation of ZrO<sub>2</sub> into the oxide coating. However, at the higher voltage (65 V), growth parameters are decreased significantly owing to both local joule heat effect and of the presence of more number of  $Zr^{2+}$  ions that competes with aluminium oxide deposition. In addition to this, dissociation of sodium oxalate has also been accelerated at higher applied voltage. The pH of the solution is increased from 8 to 9 due to the release of  $Na^+$  ions that in sequence favours the coating dissolution. When the anodising voltage is 65 V, there is a high degree of hydration and ion incorporation into the anodic coating.

## 3. 1. 3. Effect of Temperature

Fig. S1c illustrates the influence of anodising temperature on the properties of the coating when anodisation is carried out at a constant voltage of 55 V under zirconium silicate concentration at various temperatures (20° to 35 °C). When anodisation is carried out at low temperature (at 20 °C), both rates of deposition of oxide coating and its dissolution are slowed down. Therefore, at this low temperature (≤ 20 °C), the desired thickness is not achieved. When the temperature of the electrolyte increased (35°  $\pm$  1 °C) the growth properties of the coating condition, the heat produced is not disseminated efficiently and distributed uniformly throughout the electrolyte. The nucleation and the growth of the coating are not favoured and afterward, the coating starts to dissolve chemically. Ultimately, burning or breaking of the coating in the highly heated solution which leads to a decrease in thickness. It is worth mentioning that unlike conventional sulphuric acid anodisation, the process employed here does not require ice-cold conditions, thereby making the process simple. Since anodisation temperature straightforwardly influences the rate of mass transfer of O<sup>2-</sup> and Al<sup>3+</sup> ions and inward diffusion of O<sup>2-</sup> ions are assisted when the temperature is increased beyond room temperature.

#### 3. 1. 4. Effect of Process Dduration

Fig. S1d shows the effect of duration 30 min, 60 min, 90 min of anodising process on coating properties when the reaction is carried out under applied voltage of 55 V at 30 °C using electrolyte bath comprising 0.3 g/L zirconium silicate additive in 1.0 M sodium oxalate. At the beginning step, anodised layers formation prevail over the chemical dissolution of it and in compliance with Faradays' law growth kinetics of the anodised layer which is a linear dependence on anodising period. As the duration of the anodising process is prolonged beyond 30 min, aluminium reacted with oxide ions and there is a weight gain in the coating because the rate of deposition is directly proportional to process duration. This oxide coating continues to grow up to a definite period (60 min) to cover the entire surface. Accordingly, when anodisation is performed for 90 min, the thickness of the coating went down attributable for cracking or breaking of the coating. Inefficient dissipation of the amount of heat evolved during the process

is the underlying reason for this behaviour. For example, the thickness of the coating is determined to be 60  $\mu m$ , 70  $\mu m$  and 68  $\mu m$  for 30 min, 60 min, and 90 min respectively. These results exemplify the significance of the optimal duration of the anodising process. Based on the aforementioned studies and observations, the anodisation process carried out at room temperature (35°  $\pm$  1 °C) using 1.0 M sodium oxalate and 0.3 g/L zirconium silicate bath under an applied voltage of 55V for 65 min is determined to be the optimal condition.

## 3. 2. Micro-structural Analysis

### 3. 2. 1. XRD

Fig.1 shows the X-ray diffraction pattern of aluminium without additive (SO) and with additives for Zr1, Zr2, Zr3 and Zr4 samples. The pristine SO shows peaks at 17° (101), 18° (102), 23° (106), 26° (113), 30° (204), 42° (109), 51° (204), 62° (325), 87° (204) and 95° (204) which confirmed the presence of monoclinic structure. However, the addition of zirconium silicate at a constant current density exhibits the peaks located at 38°, 63° and 74° with preferred orientation of (109), (326) and (337) respectively. In the case of other additive concentration, there is little variability in peak position and depicted clearly in Fig. 2. The observed peaks are well-matched with the standard data (JCPDS card No: 88-1609). The  $\delta$ -Al<sub>2</sub>O<sub>3</sub> phase is observed for these compositions. Based on the anodising conditions, the coatings formed are mainly crystalline. It is found that the coatings after the addition of additives show some traces of zirconia and alumina. Using the Debye-Scherer equation, the average crystalline size for SO, Zr1, Zr2, Zr3 and Zr4 were 26.8 nm, 22.3 nm, 20.18 nm, 18.7 nm and 21.55 nm respectively.

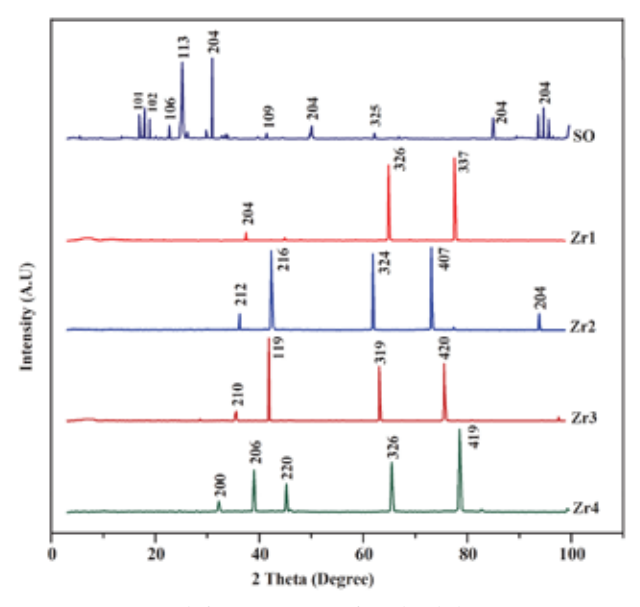


**Figure 1.** X- ray diffraction pattern of anodized aluminium coating comprising SO, Zr1, Zr2, Zr3 and Zr4.

## 3. 2. 2. Microstructure and Composition of the Coating

Microstructures related to SO, Zr1, Zr2, Zr3 and Zr4 coating are represented by Fig. S2 that depicts the differences in the morphological features. Fig. S2 of SO portrays distinctly dissimilar morphological characteristics from that of Fig S2 (b-d) which are associated with SO, Zr1, Zr2, Zr3 and Zr4 coating. SO microstructure exhibited the pores of different dimension that is formed as a result of hydrogen evolution during the process in addition to the many cracks that are visible which are formed due to the drying shrinkage. When zirconium silicate is introduced into the electrolyte, the coating becomes smoother and denser. The pores of different shapes are distributed all over the surface of the specimen after introducing the additive. Noticeably dissimilar surface morphologies prove that the addition of zirconium silicate into the electrolyte has a greater control over determining the surface morphology of the coatings. As the zirconium silicate concentration becomes higher (0.4 g/L), aluminium will be consumed at a higher rate near the bottom of the pore which is allowing continued growth of the porous layer.

The surface of Zr1, Zr2, Zr3 and Zr4 coating is smooth which is beneficial to resist the corrosion. Change in the morphology has been observed when the concentration of zirconium silicate was increased (0.3 g/L) even beyond the optimal level. Micro-sized fissures are detected with Zr4, which are created as a result of the local heating effect on the surface produced because of uneven electric field distribution and detained breakdown of the oxide layer. At lower zirconium silicate concentrations (0.1 g/L and 0.2 g/L) pores are formed along with the surfaces of micro-cracks. Only under the optimal concentration (0.3 g/L), the compact homogenous microstructure is developed. These results illustrate that the presence of zirconium silicate and its concentration are influential components that determine the morphology and properties of the coating.

#### 3. 3. SEM Cross-sectional Studies

The cross-sectional SEM images of the SO and Zr3 are represented in Fig. 2. The thickness was measured from the cross-sectional images. The average thickness of the SO and Zr3 is 5.1  $\mu m$  and 8.2  $\mu m$ , respectively. It could be visibly inferred that the quality and thickness of the coating has been improved by adding zirconium silicate into the electrolyte bath. Closer examination of images reveals that a thin deposited layer of about 1 to 1.2  $\mu m$  thickness comprising three distinct regions such as a dense barrier section at the Al /oxide interface, centre porous section followed by a columnar part of the outer surface. The outward growth of layer and retarded dissolution rate are the possible reasons for enhanced thickness value (82  $\mu m$ ) exhibited by Zr3.

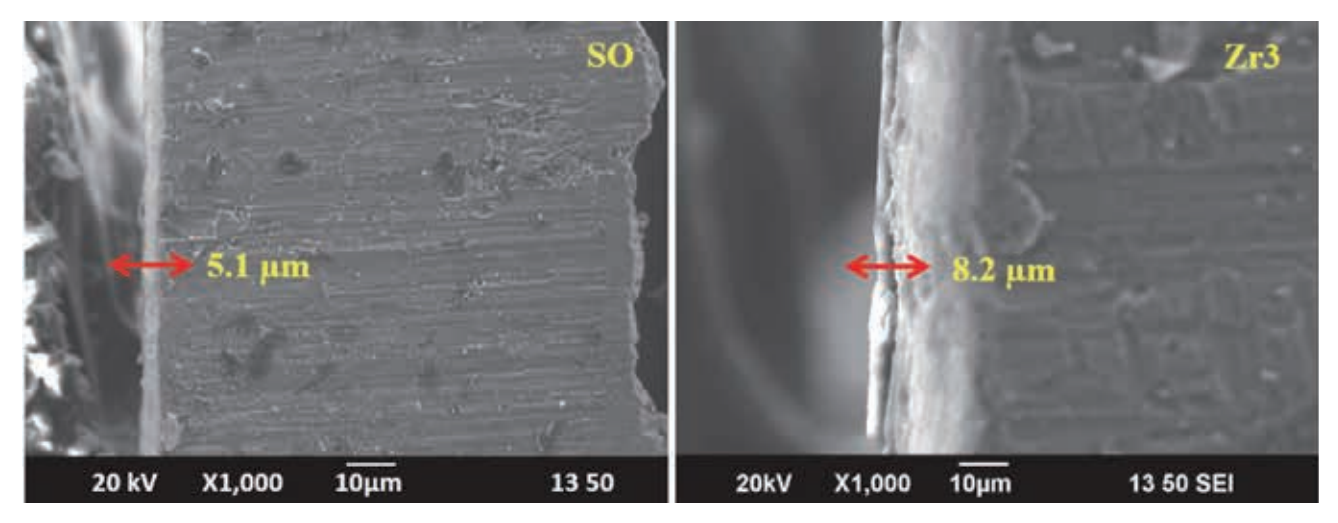


Figure 2. Cross-sectional SEM images of SO, and Zr3 coating

## 3. 4. EDS Analysis

The elements present in the various specimens are analysed by EDS spectra. Fig. S3 shows EDS spectrum of the SO and Zr3 in which both are fabricated in sodium oxalate electrolyte with the absence of additive and with the presence of optimal content (0.3g/L) of zirconium silicate additive. Aluminium and oxygen are the main constituents that are present in SO and Zr3 at 1.486 Kev (71.4 wt. % for SO and 55.8 wt. % for Zr3) and 2.307 Key (27.2 wt. % that for SO and 39 wt. % for Zr3). In contrast, the EDS spectrum of Zr3 shows well-defined peaks for Zr and Si at 4.508 Kev and 0.525 Kev respectively. This reveals the incorporation of the additive into the coating. Similarly, the weight percentage of aluminium and oxygen in sample SO are found to be 71.4% and 86.4% respectively. Whereas, in the case of Zr3 sample, the weight percentage of both elements decreases to 55.8% and 39%. The existence of Zr and Si (0.6 wt. % and 0.3 wt. %), which evidences the role of additive towards the facilitating formation of the compact and mechanically stable coating.

### 3. 5. Studies on Micro Hardness

Micro hardness associated with bare aluminium, SO, Zr1, Zr2, Zr3 and Zr4 samples are measured using Vickers micro hardness tester and are represented in the Fig S4. The average micro hardness values associated with Zr1 (0.1 g/L), Zr2 (0.2 g/L), Zr3 (0.3g/L) and Zr4 (0.4g/L) are 372 HV, 381 HV, 410 HV and 393 HV respectively. The micro hardness value increases with the concentration of zirconium silicate from 0.1g/L to 0.4g/L and then decreases. The maximum micro hardness value (410 HV) is obtained for 0.3 g/L concentration. This is related to the change in surface morphology of the coating when zirconium silicate is incorporated into the electrolyte. These silica particles are helpful in preventing the generation of

dislocations, the spread of cracks and in restraining grain boundary slides, which eventually resulted in improved mechanical properties. In addition, the increased driving force experiences at the metal / oxide interface, which promotes the reactions and on this account, the defect is formed over the surface.

# 3. 6. Studies on Corrosion Resistance of Anodised Layers

Electrochemical corrosion characteristics of SO, Zr1, Zr2, Zr3, Zr4 samples under investigation are relatively assessed by Tafel polarisation and electrochemical impedance spectroscopy (EIS) techniques in 3.5% NaCl solution.

#### 3. 6. 1. Tafel Polarisation Studies

In a 3.5% NaCl solution, the potentiodynamic polarisation behaviour of different coatings and bare aluminium is shown in Fig. 3. Table. S1 summarizes the parameters obtained by fitting the potentiodynamic curves. It can be deduced from the Fig.3 that the corrosion potential of in anodic region associated with SO, Zr1, Zr2, Zr3 and Zr4 coating display a drastic shift in the direction of the positive potential as compared to bare aluminium (-0.699V) illustrating the enhanced corrosion resistance of the coating. I<sub>corr</sub> is associated with bare aluminium is highest. (27  $\times$  10<sup>-4</sup>  $\mu A$  cm<sup>-2</sup>) but due to passivation of the anodised samples which exhibit low Icorr values as evident from Table. S1. I<sub>corr</sub> is determined to be low for the Zr3 specimen demonstrating its better corrosion-resistance. The observed values are consistent with earlier literature reports.31-33

The corrosion resistance of the Zr3 (6.70  $\times$   $10^4~\Omega$  cm $^{-2}$ ) is high compared to SO (1.51  $\times$   $10^4~\Omega$  cm $^{-2}$ ), Zr1 (2.19  $\times$   $10^4~\Omega$  cm $^{-2}$ ), Zr2 (2.35  $\times$   $10^4~\Omega$  cm $^{-2}$ ) and Zr4 (6.44  $\times$   $10^4~K\Omega$  cm $^{-2}$ ). The corrosion resistance of the coating

increases with the concentration of zirconium silicate up to 0.3 g/L and after that begins to decline. These results are compliant with the open circuit potential values. This shows that the incorporation of zirconium silicate into the electrolyte bath imparts mechanical strength to the coating rather porous with smaller thickness is resulted when sodium oxalate alone is used as an electrolyte that produces a detrimental effect on its corrosion resistance. The difference in the resistance and polarisation behaviour is mainly owing to the structure and morphology of the coating. Since the corrosion rate depends on the coating thickness, the coating with lower thickness and high porous nature will undergo the corrosion readily due to uncomplicated accessibility of destructive ions. However when zirconium silicate is incorporated with sodium oxalate electrolyte, both pores size and the number of pores decreased. By increasing the concentration of zirconium silicate additive, highly thick non-porous morphology has been formed that helps to acquire more corrosion-resistant property due to the restricted penetrations of corrosive ions into the coatings.

This type of coating is generated when the optimal zirconium silicate concentration (0.3 g/L) is maintained during anodisation at appropriate temperature and voltage. However, when zirconium silicate concentration is exceeded above 0.3 g/L, the thickness is reduced through modified rate of deposition and perceptibly and the corrosion potential decreases. As a result of their lower corrosion current densities, thicker coatings with less porous nature reflect higher corrosion resistance. On the other hand, shape and porosity, not just thickness, have a significant effect in determining the specimen's corrosion resistance.

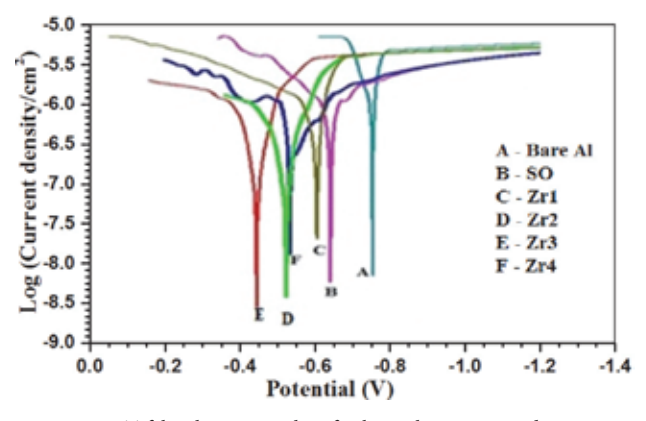


**Figure 3.** Tafel polarization plots for bare aluminium and various anodized coating immersed in 3.5% NaCl solution (a) bare Al, (b) SO, (c) Zr1, Zr2, Zr3 and Zr4.

## 3. 6. 2. Electrochemical Impedance Studies

EIS measurements were performed with bare aluminium, SO, Zr1, Zr2, Zr3 and Zr4 coating to distinguish the corrosion kinetics across the modified coating and

substrate interface of aluminium specimens Fig. 4 and Fig. 5 show an electrical equivalent circuit model used in this study for the fitting analysis, which is a simplified electrochemical model that has been consistently reported for the comparative Nyquist of SO, Zr1, Zr2, Zr3 and Zr4 samples in 3.5% of NaCl obtained at open circuit potential after immersion of the samples for 500s. Based on the equivalent circuit model proposed, these EIS curves were best fitted and the resulting parameters are tabulated in Table. 1. R<sub>p</sub> represents a measure of corrosion resistance that indicates the extent of protection against corrosion and is inversely proportional to I<sub>corr.</sub> Like the Tafel polarisation studies, EIS data also indicate that corrosion resistance improved, substantially after anodising as compared to the bare aluminium ( $R_f$ : 3011  $\Omega$  cm<sup>-2</sup>;  $C_{dl}$ : 11.25 $\mu$ Fcm<sup>-2</sup>). Fascinatingly, the coating generated on the surface that plays a dual role in preventing corrosion both through decreasing rate of charge transfer process and diffusion across the surface layer. From Table.1 it is apparent that Zr4 (1607  $\Omega$  cm<sup>-2</sup>) samples display high resistance compared to other samples under study, which demonstrates a role of silicate additive towards protecting surface corrosion. It is implied that water and electrolytic solution penetrate through the anodic layer which composed of larger pores to initiate the corrosive attack in case of the thin layered SO sample, but Zr1, Zr2, Zr3 and Zr4 samples comprising dense, close-packed network restricts the penetration of corrosive ions through them.  $R_p$  and  $C_{dl}$  are noted to be minimised for Zr3 layer, which is due to a diminution in local dielectric constant and/or to an increase in electrical double layer thickness.

On comparing passivation current densities, it is inferred that the anodic coating obtained using sodium oxalate-zirconium silicate electrolyte provides an excellent barrier for defending against corrosion. The features of the coating are reflected by the high-frequency section of the

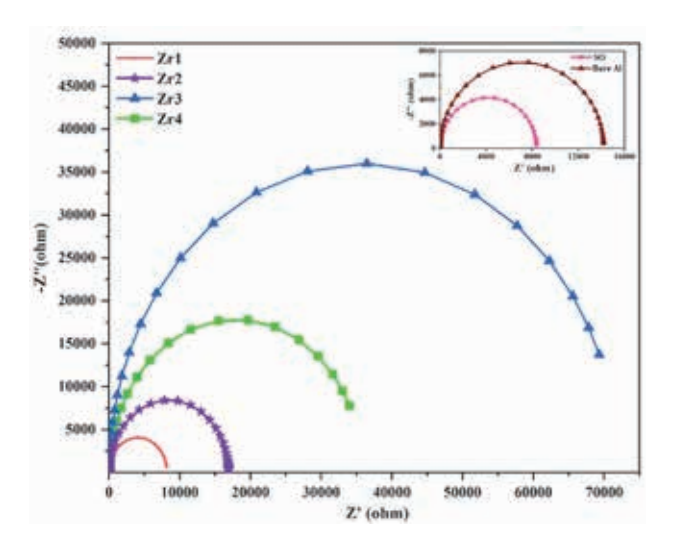


**Figure 4.** Nyquist plot curves associated with bare aluminium and various anodized aluminium coating immersed in 3.5% NaCl solution Zr1, Zr2, Zr3 and Zr4 anodic layers. Inset of figure shows that of bare Al and SO.

spectrum, while the lower portion of the spectrum is connected to the Faradic reaction occurring on the aluminium surface, according to the literature.  $^{24-25}$  EIS of SO is different from that of all other samples which are consistent with the formation of a stable passive layer on these surfaces. Low capacitance that arises owing to strong interaction of small organic molecules on the surface that results in poor dissolution reaction. The surface homogeneity of coating also helps to develop good corrosion resistance, which higher resistance ( $R_f$ ) compared to bare aluminium. By restricting the access of aggressive ions causing corrosion.  $^{26-30}$ 

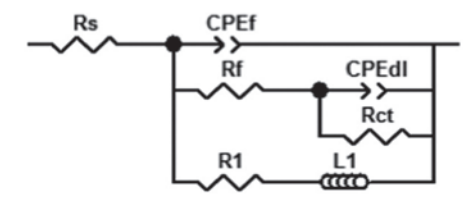


**Figure 5.** An electrochemical equivalent circuit model fitted for impedance data analysis of anodized aluminium layers in this study.

#### 3. 6. 3. Wettability Studies

The aforementioned studies confirm that Zr3 exhibits suitable surface and further it is subjected to hydrophobic treatment. It can be seen from Fig. 6 that contact angle (CA) associated with the anodised aluminium surface. After Stearic acid 3 g/L immersion, the contact angle of Zr3 is increased to  $122^{\circ} \pm 0.4^{\circ}$  for 15 min (SA1) treatment. When the specimen is further subjected to KOH 10 g/L treatment the contact angle is increased to  $152.76^{\circ} \pm 0.4^{\circ}$  (SA2). Among SA1 and SA2, the SA2 sample shows a higher contact angle. The wettability of a solid surface is strongly affected by both surface structure and chemical composition.<sup>34</sup>

## 3. 6. 4. Studies on Corrosion Behaviour of Hydrophobic Surface SA1 and Superhydrophobic Surface SA2

To examine the corrosion resistance of the hydrophobic coating corrosion studies were carried out for Zr3, SA1 and SA2 samples for comparison. The results are shown in Fig. S5 and Fig. S6. Fig. S5 shows the Tafel polar-

**Table 1.** Corrosion parameters derived from EIS Nyquist plot analysis associated with bare aluminium, SO and various Zr3 anodic layers under applied voltage of 45 V for 65 min at room temperature.

Sample	CPE <sub>f</sub> (μF cm <sup>-2</sup> )	R <sub>F</sub> (Ohm cm <sup>2</sup> )	CPE <sub>dl</sub> (μF cm <sup>-2</sup> )	R <sub>ct</sub> (Ohm cm <sup>2</sup> )	R <sub>1</sub> (Ohm cm <sup>2</sup> )
Bare Al	11.25	3011	198	1765	1298
SO	8.21	1023	209	1613	1267
Zr1	7.43	879	221	1658	1109
Zr2	6.02	674	227	1654	979
Zr3	5.45	476	238	1607	875
Zr4	5.77	489	241	1605	889

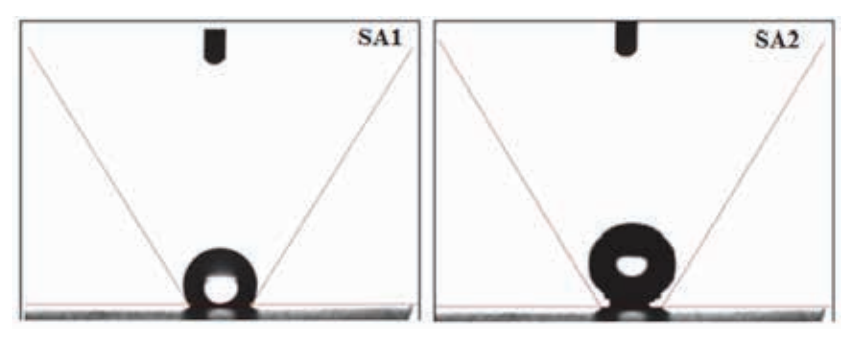


Figure 6. Effect of various treatment duration on contact angle of the coating.

**Table 2.** Corrosion parameters derived from EIS Nyquist plot analysis associated with SA1 and SA2.

Sample	CPE <sub>f</sub> (μF cm <sup>-2</sup> )	R <sub>F</sub> (Ohm cm <sup>2</sup> )	CPE <sub>d</sub> (μF cm <sup>-2</sup> )	R <sub>ct</sub> (Ohm cm <sup>2</sup> )	R <sub>1</sub> (Ohm cm <sup>2</sup> )
SA1	8.5	438	217	1564	778
SA2	7.8	341	252	1245	651

isation curves for SA1 and SA2. Among all samples SA2 shows low  $I_{corr}$  (6.04  $\times$   $10^{-8}~\mu A/cm^2)$  and high  $E_{corr}$  (–0.02 V) shifts towards a more positive direction compared to SA1 ( $I_{corr}$ : 7.01  $\times$   $10^{-7}~\mu A/cm^2$ ;  $E_{corr}$ : –0.321 V) and Zr3

 $(I_{corr}: 6.14 \times 10^{-7} \,\mu\text{A/cm}^2; \, E_{corr}: -0.428 V)$  as shown by Table S2. The obtained result shows that in the instance of SA2, chloride ion (Cl<sup>-</sup>) transport may have been severely hindered. This demonstrates that a covering with a larger

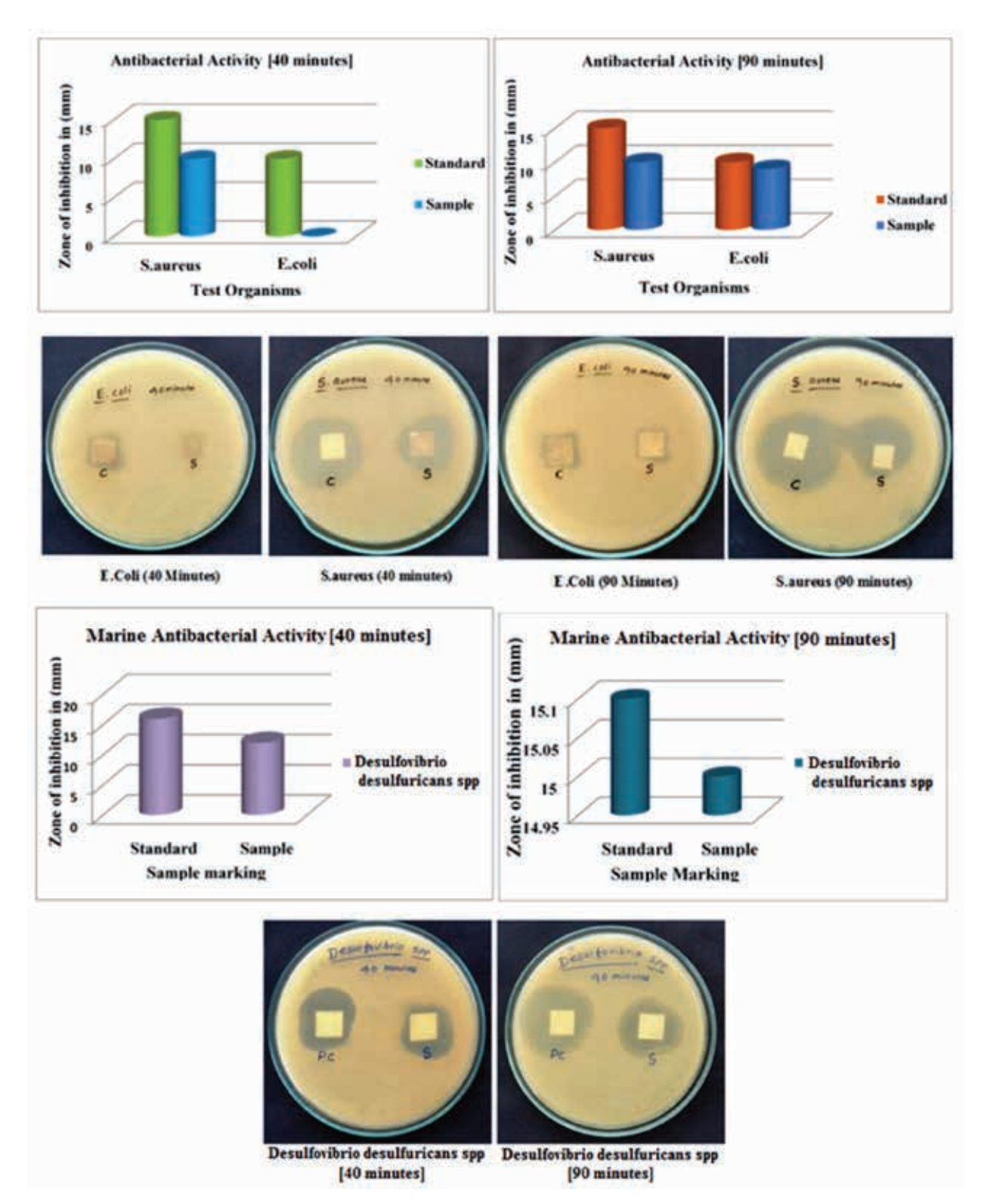


Figure 7. Marine antibacterial activities of Zr3 specimens tested with S.Aureus, E.Coli and D.desulfuricans.

contact angle inhibits corrosion better. Here SA2 has a higher contact angle than SA1 and Zr3. Two key elements might be responsible for the increased corrosion resistance mechanisms. For starters, the SA2 is made up of hierarchical micro-nanostructures that may readily trap significant volumes of air within the coating's micro-/nano-pores. The trapped air acts as a passivation layer, protecting the aluminium substrate from Cl attachment. Water transport against gravity is simple in a porous surface structure with a CA greater than 150°. Therefore, the NaCl solution can be pushed out from the pores of the SA1 by the pressure and the aluminium substrate could be effectively protected. Hence, the structure and properties are influence directly to its corrosion behaviour as exemplified by Tafel studies. Fig. S6 shows the impedance plots of Zr3, SA1, and SA2. Like Tafel studies, the SA2 sample shows higher corrosion resistance than other sample SA1 and Zr3. This model has been proposed for analysis of superhydrobhobic aluminium surface previously by recent researchers.<sup>35–39</sup>

### 3. 6. 5. Marine Bacterial Activity

The bacterial activity of Zr3 coating was tested against E.coli, S. aureus, and marine bacterial strain namely, D. desulfuricans for 24 h, which is shown in Fig. 7. From the results, it is shown that the zone of inhibition for Zr3 against S.aureus strains and D. desulfuricans is 10 mm (40 min), 12 mm (90 min). The zone of inhibition against D. desulfuricans is increased from 12 mm (40 min) to 15 mm (90 mm) respectively. The results show that the D. desulfuricans bacteria demonstrated higher activity than E.coli and S. aureus due to the minimal solid-liquid contact at the surface, weak surface interactions with bacteria, and low surface energy. The key to the antibacterial qualities is the self-cleaning concept, which allows for easy washing and eliminates the need for antibacterial chemicals. Due to the fact that this antibacterial design is simply structural, a product with permanent characteristics may be created for everyday use with minimum customer maintenance.

## 4. Conclusions

In conclusion, this work reports on the fabrication of the coatings by anodisation of aluminium in 0.1M sodium oxalate with and without the addition of zirconium silicate. The results revealed that experimental conditions such as additive concentration, applied voltage, process time and temperature play a crucial role in coating formation and tailoring of their surface properties which increases the thickness, growth rate, and micro hardness up to a certain concentration (0.3 g/L; Zr3) and then decreases. The maximum thickness (82 µm), growth rate (1.2 µm/ min), and micro hardness (410HV) are obtained at the voltage of 55V in room temperature (35  $\pm$ 1 °C) for 60 min. The SEM and EDX results demonstrate that the addition of zirconium silicate into the electrolyte has an impact on the morphology as it favours the formation of dense and uniform coating with fewer structure imperfections. The XRD studies confirmed the presence of  $\delta$  alumina. Our studies further show that the coating formed with the addition of zirconium silicate has more corrosion resistance (6.70×10<sup>4</sup>  $\Omega$  cm<sup>-2</sup>) when compared to the sodium oxalate electrolyte (1.0 M) alone as an electrolyte. To extend its applications in the marine field, the surface of the Zr3 sample is modified to superhydrophobic (SA2). The superhydrophobic (SA2) sample shows higher corrosion resistance (1.68 x108  $\Omega$  cm<sup>-1</sup>), which is higher than the Zr3 sample (6.8 × 10<sup>3</sup>  $\Omega$ cm<sup>-1</sup>). The contact angle of the coating for the SA1 and SA2 sample is found to be  $122^{\circ} \pm 0.4^{\circ}$  and  $152.76^{\circ} \pm 0.4^{\circ}$ . This contact angle of super hydrophobic coating is improved owing to base (KOH) treatment. The marine applications and microbial activity were investigated against S. aureus (40 min: 10 mm; 90 min: 12 mm) and D.desulfuricans (40 min: 12 mm; 90 min: 15 mm). Thus the fabricated coating is compatible with industrial, biological, biomedical, optical, and aerospace applications with the specifically focused utility to mitigate the marine corrosion.

## 5. References

E. W. Lee, T. Oppenheim, K. Robinson, B. Aridkahari, N. Neylan, D. Gebreyesus, M. Richardson, M. Arzate, C. Bove, M. Iskandar, C. Sanchez, E. Toss, I. Martinez, D. Arenas, J. Ogren, J. Mclennan, R. Clark, W. E. Frazier, O. S. Es-Said, *Eng. Fail. Anal.*, 2007, *14*, 1538–1549.

DOI:10.1016/j.engfailanal.2006.12.008

M. G. Mueller, M. Fornabaio, G. Zagar, A. Mortensen, *Acta Mater.*, 2016, 105, 165–175. DOI:10.1016/j.actamat.2009.11.043

**Table 2.** Zone of inhibition exhibited by Zr3 towards S.Aureus, E.Coli and D.desulfuricans for incubation period of 40 min and 90 min.

S.No.	Test Organisms	Zone of inhibition in (mm) on 40 min		Zone of inhibition in (mm) on 90 min	
		Control	Sample	Control	Sample
1	S. aureus	15mm	10mm	15mm	12mm
2	E.coli	10mm	HA	10mm	9mm
3	D. desulfurican	15mm	12mm	16mm	15mm

- A. Ghahremaninezhad, A. Dolati, J. Alloys Compd., 2009, 480, 275–278. DOI:10.1016/j.jallcom.2009.02.020
- 4. J. Bajat, I. Milosev, Z. Jovanovic, R. M. Jancic-Heinemann, M. Dimitrijevic, *Corros. Sci.*, **2010**, *52*(*3*), 1060–1069. **DOI:**10.1016/j.corsci.2009.11.035
- E. Matykina, R. Arrabal, A. Mohamed, P. Skeldon, G. Thompson, *Corros. Sci.*, 2009, 51(12), 2897–2905.
  DOI:10.1016/j.corsci.2009.08.004
- V. Raj, M. Mubarak Ali, J. Mater, *Proc. Tech.*, 2009, 209(12-13), 5341–5352. DOI:10.1016/j.jmatprotec.2009.04.004
- K. Xhanaria, M. Finšgar, RSC Adv., 2016, 6, 62833.
  DOI:10.1039/C6RA11818F
- 8. I. Milošev, *Acta Chim. Slov.*, **2019**, *66*, 511. **DOI**:10.17344/acsi.2019.5162
- B. Kuznetsov, M. Serdechnova, J. Tedim, M. Starykevich, S. Kallip, M. P. Oliveira, T. Hack, S. Nixon, M. G. S. Ferreira, M. L. Zheludkevich, *RSC Adv.*, **2016**, *6*(17), 13942–13952.
  **DOI:**10.1016/j.jallcom.2014.12.176
- 10. S. Zhang, Q. Xu, Z. Wang, S. Hao, C. Sun, W. Ma, *Surf. Coat. Technol.*, **2018**, *346*, 48–52. **DOI:**10.1021/jp0560664
- 11. Z. Wang, Q. Li, Z. She, F. Chen, L. Li, J. Mater. Chem., 2012, 22(9), 4097–4105. DOI:10.1039/c2jm14475a
- 12. Y. Lai, X. Gao, H. Zhuang, J. Huang, C. Lin, *Adv. Mater.*, **2009**, 21(37), 3799–3803. **DOI**:10.1002/adma.200900686
- S. Jung, M. Dorrestijn, D. Raps, A. Das, C.M. Megaridis, D. Poulikakos, *Langmuir.*, 2011, 27(6), 3059–3066.
  DOI:10.1021/la104762g
- Z. She, Q. Li, Z. Wang, C. TaN, J. Zhou, L. Li, Surf. Coat. Technol., 2014, 251, 7–14. DOI:10.1016/j.surfcoat.2014.03.060
- J. Y. Huang, S. H. Li, M. Z. Ge, L. N. Wang, T. L. Xing, G. Q. Chen, X. F. Liu, S. S. Al-Deyab, K. Q. Zhan, T. Chen, Y. K. Lai, *J. Mater. Chem.*, A. 2015, 3(6), 2825–2832.
  DOI:10.1039/C4TA05332J
- H. Kim, K. Noh, C. Choi, J. Khamwanna, D. Villwock, S. Jin, Langmuir., 2011, 27(16), 10191–10196.
   DOI:10.1021/la2014978
- J. Yu, L. Qin, Y. Hao, S. Kuang, X. Bai, Y. M. Chong, W. Zhang, *ACS Nano.*, 2010, 4(1), 414–422.
   DOI:10.1021/nn901204c
- 18. B. Qian, Z. Shen, *Langmuir.*, **2005**, *21*(2), 9007–9009. **DOI:**10.1021/la051308c
- A. V. Rao, S. S. Latthe, S. A. Mahadik, C. Kappenstein, *Appl. Surf. Sci.*, 2011, 257(13), 5772–5776.
  DOI:10.1016/j.apsusc.2011.01.099

- 20. A. Chaudhary, H. C. Barshilia, *J. Phys. Chem. C.*, **2011**, *115(37)*, 18213–18220. **DOI**:10.1021/jp204439c
- J. Li, Z. Jing, Y. Yang, Q. Wang, Z. Lei, Surf. Coat. Technol.,
  2014, 258,973–978. DOI:10.1016/j.surfcoat.2014.07.047
- C. Dong, Y. Gu, M. Zhong, L. Li, K. Sezer, M. Ma, *J. Mater. Process. Technol.*, 2011, 211(7), 1234–1240.
  DOI:10.1016/j.jmatprotec.2011.02.007
- T. Darmanin, E. T.de Givench, S. Amigoni, F. Guittard, *Adv. Mater.*, 2013, 25(10), 1378–1394.
  DOI:10.1002/adma.201204300
- H. Wang, D. Dai, X. Wu, Appl. Surf. Sci., 2008, 254(17), 5599–5601. DOI:10.1016/j.apsusc.2008.03.004
- 25. W. Liu, Y. Luo, L. Sun, R. Wu, H. Jiang, Y. Liu, *Appl. Surf. Sci.*, **2013**, *264*, 872–878. **DOI:**10.1016/j.apsusc.2012.10.167
- R. Jafari, R. Menini, M. Farzaneh, *Appl. Surf. Sci.*, 2010, 257(3), 1540–1543. DOI:10.1016/j.apsusc.2010.08.092
- S. Peng, W. Deng, Colloids. Surf., A. 2015, 481, 143–150.
  DOI:10.1016/j.colsurfa.2015.04.037
- 28. D. Ma, S. Li, C. Liang, *Corros. Sci.*, **2009**, *517*, 713. **DOI:**10.1016/j.jmrt.2020.08.085
- 29. V. Raj, M. Mubarak Ali, *J.Mater. Proc. Tech.*, **2009**, *209*(*12-13*), 5341–5352. **DOI**:10.1016/j.jmatprotec.2009.04.004
- V. Zinkevich, I. Bogdarina, H. Kang, M. A. W. Hill, R. Tapper,
  I. B. Beech, *Int. Biodeterior. Biodegrad.*, 1996, 37(3-4), 163–172. DOI:10.1080/08927019909378396
- 31. M. Mubarak Ali, S. Sathiya, *Curr. Sci.*, **2020**, *118*(2), 234. **DOI:**10.18520/cs/v118/i2/234-242
- 32. H. Ji, G. Chen, J. Yang, J. Hu, H. Song, Y Zhao, *Appl. Surf. Sci.*, **2013**, *266*,105. **DOI**:10.1016/j.apsusc.2012.11.103
- 33. V. Raj, M. Mumjitha, *Mater. Sci. Eng. B.*, **2014**, (*179*), 25–35. **DOI:**10.1016/j.mseb.2013.10.001
- 34. S. Senbahavalli, S. Mohanapriya, V. Raj, *Materials Discovery*, **2016**, *(3)*, 29–37. **DOI:**10.1016/j.md.2016.08.001
- G. S. Hikku, K. Jeyasubramanian, A. Venugopal, R. Ghosh, J. Alloys and Compounds., 2017, (716), 259–269.
  DOI:10.1016/j.jallcom.2017.04.324
- 36. D. Zang, R. Zhu, W. Zhang, J. Wu, X. Yu, Y. Zhang, *Corros. Sci.*, **2020**, *(83)*, 86–93. **DOI**:10.1016/j.corsci.2014.02.003
- Y. Huang, D. K. Sarkar, X. G. Chen, Appl. Surf. Sci., 2015, 356, 1012–1024. DOI:10.3390/ma12010109
- 38. H. A. Sorkhabi, S. A. Nabavi, Acta Chim. Slov. 2000, 47, 507.
- 39. M. Lalić, S. Martinez, *Acta Chim. Slov.* **2019**, *66*, 513–522. **DOI:**10.17344/acsi.2019.5113

## **Povzetek**

V tem delu smo preučili anodizacijo aluminija v 1.0 M raztopini natrijevega oksalata in metodološko ovrednotili vpliv cirkonijevega silikata kot aditiva. Podrobneje smo preučili vpliv aditiva na strukturo, morfologijo, mikrotrdoto in sestavo prevleke pod različnimi pogoji anodizacije. Površina prevleke je bila obdelana s stearinsko kislino, čas stika prevleke s kislino pa je bil optimiziran. Poleg že navedenega smo preučili tudi odvisnost morfologije površine, kinetskih parametrov in mikrostrukturnih lastnosti prevleke od elektrolita oziroma koncentracije aditiva, časa anodizacije in temperature. Analize z rentgensko praškovno difrakcijo (XRD) in vrstično elektronsko mikroskopijo (SEM), kombinirano z energijskodisperzijsko spektroskopijo (EDS), so pokazale ugoden vpliv aditiva na nastanek kristalinične prevleke z izboljšanimi protikorozijskimi lastnostmi. Prevleke z aditivom so superhidrofobne. Z namenom povečanja statičnega kontaktnega kota vode, ki je znašal  $122^{\circ} \pm 0.4^{\circ}$ , so bile prevleke z aditivom obdelane s KOH, kar je pod najugodnejšimi pogoji kot povečalo na  $152.76^{\circ} \pm 0.4^{\circ}$ . Pri tem kotu je korozijska upornost sistema znašala  $1.68 \times 10~\Omega$  cm<sup>-1</sup>, kar je skoraj osemkrat več kot pri čistem aluminiju ( $8.36 \times 10^{1}~\Omega$  cm<sup>-1</sup>). Prikazana je tudi učinkovitost tovrstnih površinsko modificiranih prevlek proti trem različnim vrstam bakterij; morski bakteriji *Desulfovibrio desulfuricans* in medicinsko relevantnima bakterijama *Staphylococcus aureus* ter *Escherichia coli*.



Except when otherwise noted, articles in this journal are published under the terms and conditions of the Creative Commons Attribution 4.0 International License